Synthetic Metals 196 (2014) 186–192

Contents lists available at ScienceDirect

Synthetic Metals

journal homepage: www.elsevier.com/locate/synmet

The effect of compressive stress on the electrically resistivity of poly(vinylidene fluoride)/polypyrrole blends

Claudia Merlini[a,b], Guilherme Mariz de Oliveira Barra[a,*], Thiago Medeiros Araujo[b], Alessandro Pegoretti[b,*]

[a] Mechanical Engineering Department, Federal University of Santa Catarina (UFSC), Florianópolis, SC, Brazil
[b] Department of Industrial Engineering, University of Trento, 38123 Trento, Italy

ARTICLE INFO

Article history:
Received 11 May 2014
Received in revised form 26 July 2014
Accepted 2 August 2014

Keywords:
Pressure sensor
Polypyrrole
Poly(vinylidene fluoride)
Conducting blends

ABSTRACT

Variation of the electrical resistivity under repeated loading–unloading compressive cycles of poly(vinylidene fluoride) (PVDF)/polypyrrole (PPy) blends prepared by solution-casting has been investigated. The insulator–conductor transition of the PVDF/PPy blends was very sharp and the percolation threshold was found to be below 4 wt%. PVDF/PPy blends exhibits a decrease in the electrical resistivity with the applied compressive stress due to the formation of new conducting pathways. Electromechanical response was dependent of PPy amount and the maximum sensitivity was obtained for a blend with a PPy content of 9 wt%, for which the electrical resistivity drops by two orders of magnitude, e.g. from 10^8 to 10^6 Ω cm. The electrical resistivity variation during compressive stress cycles, the reproducibility and the reversibility makes this system a suitable material for the development of pressure sensors.

1. Introduction

Piezoelectric sensors based on poly(vinylidene fluoride) (PVDF) have been successfully obtained and described by several authors [1–5]. These systems are commonly used in piezoelectric devices to measure forces and strains, corresponding to micron-scale motions, especially those of dynamic nature, such as vibrations, accelerations and oscillations [6]. Such devices present high sensitivity in the low pressure regime (<10 kPa) [2] and operate through the reorganization of crystalline dipole density (polarization vector) in response to applied stress [6]. Although PVDF have been exploited in many sensing applications, there are some limitations, e.g., the response of piezoelectric sensors can drifts due to undesirable noise and/or interference, such as mechanical vibrations, static electricity, stray capacitances and temperature changes [2]. Additionally, they have very high resistance and require high input impedance devices for further data treatment [7].

Hence, the development of semi-conductive sensors based on electrically conductive polymer composites is an interesting alternative, because these materials combine electrical conductivity, flexibility, ease of processing, associated with low cost and simplicity in device fabrication. Electrically conductive polymer composites with properties suitable for pressure sensor applications have been developed through incorporation of conductive fillers into an insulating polymer matrix, such as thermoplastic polymers or unsaturated rubbers. Among the investigated fillers we may list intrinsically conducting polymers (ICPs) [7–11] and carbonaceous fillers such as carbon black [12,13] and graphite [14]. Differently from the systems based on the piezoelectric concept, the changes of the electrical resistivity in conductive polymer composites during a loading–unloading cycle can be explained by percolation theory [15]. Under compressive stress, the dispersed conductive particles come into a closer contact to form a conducting network. However, when the compression stress is released, the conducting pathways are disrupted and the electrical resistivity returns to the initial value to that without pressure [13,16]. Alternatively, there are examples of carbon black polymer composites in which the electrical resistivity increases when compressive stress is applied due to the destruction of the conducting network [17].

Several authors have studied the electro-mechanical response of conductive polymer blends based on intrinsically conducting polymers (ICPs) which are mainly produced through solution or melt processing methods [7–9,11,18–20]. One of the main challenge in developing these materials is how to reach an adequate pressure sensitivity at low conducting filler concentration in order

* Corresponding authors at: Federal University of Santa Catarina, Mechanical Engineering, Campus Universitário, Trindade, 88037-500 Florianópolis, SC, Brazil. Tel.: +4899415094.
E-mail addresses: g.barra@ufsc.br (G.M.d.O. Barra), alessandro.pegoretti@unitn.it (A. Pegoretti).

http://dx.doi.org/10.1016/j.synthmet.2014.08.002
0379-6779/

to minimize processing complexity and depletion of the mechanical properties of the host-insulating polymer [18]. The electrical resistivity changes during loading cycles are influenced especially by the matrix structure, conducting filler concentration, processing method and interaction between both components. Additionally, most of the pressure sensitive materials have displayed some degree of hysteresis after subsequently compression cycles. Souza et al. [8] reported on the development of a pressure sensitive material based on styrene–butadiene–styrene block copolymer (SBS) filled polyaniline (PANI). Applying compressive stress up to 3.5 MPa, changes on the electrical resistivity from 5.0×10^6 to 1.0×10^6 were detected. Radhakrishnan and Kar [7] investigated the response of SBS/PANI blends prepared through solution casting method and observed that blends with 15 wt% PANI content exhibited the best electrical–mechanical performance. Kalasad et al. [19] demonstrated that the pressure sensitivity of polyaniline/*cis*-1,4-polyisoprene blends is highly influenced by the PANI content. In our previous works, we have demonstrated that the incorporation of PANI or polypyrrole (PPy) into thermoplastic elastomer is an excellent alternative to produce conducting blends with good electrical conductivity and electrical–mechanical response changes [9,18,20]. Moreover, many works in the literature have reported interesting results concerning the production and characterization of PVDF/PPy or PANI blends [21–23]; however, few of them have exploited the properties of these materials for pressure sensing applications. Radhakrishnan and Kar [24] published an interesting work describing the influence of the incorporation of HCl or DBSA doped PANI, denoted as PANI.HCl and PANI.DBSA, respectively, into PVDF matrix on the pressure sensitivity of the obtained PVDF/PANI blends. The PVDF/PANI.HCl blends with 10 wt% PANI content displayed a variation of electrical resistivity of SEBS/PANI of about one order of magnitude.

Based on the above considerations, the focus of this study is to develop PVDF/PPy blends for pressure sensing applications. The electro-mechanical response of the blends containing different weight fraction of DBSA doped PPy was evaluated. Additionally, the morphology, electrical and thermal properties were also investigated.

2. Experimental

2.1. Materials

Pyrrole (Aldrich; 98%) was distilled under vacuum and stored in a refrigerator. Iron(III) chloride hexahydrate ($FeCl_3{\cdot}6H_2O$) (analytical grade), dodecylbenzenesulfonic acid (DBSA), 70 wt% solution in 2-propanol and poly(vinylidene fluoride) (PVDF) with molecular weight (M_w) of 534 kDa were supplied by Aldrich Chemistry. Dymethylformamide (DMF) (99.8%) and acetone (99.5%) were purchased from Aldrich and Merck, respectively. With exception of the pyrrole, all materials were used without further purification.

2.2. Synthesis of PPy

The pyrrole oxidative polymerization was performed in the presence of dodecylbenzenesulfonic acid (DBSA) using ferric chloride ($FeCl_3$) as oxidant, according to Mičušík et al. [25]. First, the anionic surfactant DBSA (1.88 g) was dissolved in 0.05 L of distilled water and then 2 mL (0.3 mol L^{-1}) of pyrrole (Py) was added. After 10 min, 16.2 g of iron(III) chloride hexahydratate ($FeCl_3{\cdot}6H_2O$) dissolved in 0.05 L distilled water was slowly added. The oxidant-to-monomer molar ratio was 2/1. The polymerization was carried out for 6 h at room temperature under magnetic stirring. After the polymerization, the precipitated PPy particles were filtered and thoroughly washed with distilled water in order to extract the byproducts and residues of the reaction and vacuum dried at room temperature.

2.3. Preparation of PVDF/PPy blends

PVDF/PPy blends were prepared through solution casting technique. The PVDF was dissolved in DMF under stirring for 2 h at 70 °C. After cooling, acetone was added to the solution under stirring in a proportion DMF/acetone 75/25 in weight, resulting in a 20 wt% solution. PPy was inserted into the PVDF solution at various weight concentrations (from 3 to 23 wt%). The PVDF/PPy suspensions was mechanically stirred for 10 min and sonicated with an ultrasonic probe (Ultrasonic Processor UP400S Hielscher, 50 W and 60 Hz) for 5 min. The mixture was cast onto a glass plate to evaporate the solvent at 70 °C, resulting in conducting polymer films with thickness lower than 200 μm. The samples have been denoted as PVDF/PPy_*x*, where *x* represents the weight content of PPy in the blend.

2.4. Characterization

Electrical resistivity measurements on the PPy and PVDF/PPy blends were performed using the four probe standard method with the current applied by a Keithley 6220 source a and the potential measured through a Keithley Model 6517A electrometer. For pure PVDF and high-resistivity blends the measurements were performed using a Keithley 6517A electrometer connected to a Keithley 8009 test fixture. Sample measurements were performed at least five times at room temperature.

The microstructures of PVDF/PPy blends were analyzed by using a Zeiss—Supra 60 field emission scanning electron microscope (FESEM). The samples were sputtered with gold and observed using a secondary electron detector and applied tension between 2 and 4 kV.

Thermogravimetric analysis (TGA) was carried out using a TGA Q5000IR (TA Instruments, USA) thermo-gravimetric analyzer. The analyses were performed at 10 °C min^{-1} from 35 °C to 700 °C under a nitrogen flux of 25 mL min^{-1}.

Attenuated total reflectance-Fourier transform infrared spectroscopy (ATR-FTIR) of pure PPy, PVDF and blends were performed on a Bruker spectrometer (model Tensor 27), in the range of wavenumbers of 4000–550 cm^{-1} by accumulating 32 scans at a resolution of 4 cm^{-1}.

Differential scanning calorimetry (DSC) measurements were performed on a Mettler DSC30-TA Low Temperature and a Metler TC 15 TA Controller at a heating rate of 10 °C min^{-1}, from −75 °C to 220 °C, under a nitrogen flux of 100 mL min^{-1}. The cristallinity content (X_c) of PVDF was calculated on the basis of the following Equation:

$$X_c = \frac{\Delta H_f}{\Delta H_f^* \phi} \times 100 \quad (1)$$

where ΔH_f is the sample enthalpy of fusion, ΔH_f^* is the heat of fusion of perfectly crystalline PVDF (104.7 J g^{-1} [26]) and ϕ is the weight fraction of PVDF in the PVDF/PPy blend.

Dynamic mechanical thermal analysis (DMTA) experiments were carried on a dynamic mechanical analyzer DMA Q800, (TA Instruments) under tensile mode on rectangular specimens with a width of 6.4 mm and a length of 30 mm. The analyses were performed at a frequency of 1 Hz at a peak-to-peak displacement of 64 μm, scanning the temperature range (from −100 to 130 °C), at a heating rate of 3 °C min^{-1}.

The setup used to measure the electro–mechanical response of the PVDF/PPy blends on compressive stress, consists of an universal testing machine (Instron®, model 5969) to apply a compressive stress and a electrometer (Keithley 6517A) to acquire the

resistivity data. The specimen was placed between two electrodes (Ø = 22.5 mm) which were confined in a poly(tetrafluoroethylene) cylinder. The device was then placed between the testing plates of the universal testing machine and the electrodes were connected to the electrometer. The samples were loaded up to 5 MPa at a loading rate of 1 MPa min^{-1} and the compressive stress was released at the same loading rate. For each sample, loading–unloading sequences of 5 and 25 cycles were performed on different specimens. The electrical resistivity ρ (Ω cm) was calculated through Eq. (2), where R is the measured resistance (Ω), d is the sample diameter (cm) and w is the specimen thickness (cm).

$$\rho = \frac{\pi \times R \times d^2}{4w} \quad (2)$$

3. Results and discussion

As reported in Fig. 1(a), for the blends prepared through solution casting the electrical resistivity decreases as the PPy content increases with a sharp transition from insulative to conductive behavior. Below the percolation threshold, (e.g., at 3 wt% of PPy), the electrical resistivity of PVDF/PPy composites is quite similar to that found for neat PVDF (10^{13} Ω cm), since the PPy domains are isolated from each others in the insulating matrix (Fig. 1(b)). With increasing the PPy concentration, the electrical resistivity decreases abruptly by ten orders of magnitude, reaching an almost constant value after a PPy content of about 13 wt%. This behavior indicates the presence of a network of interconnected PPy domains in the PVDF matrix (Fig. 1(c and d)).

The experimental data presented in Fig. 1(a) has been used to estimate a percolation threshold of the system. According to the classical percolation theory, electrical resistivity of a filled material follows a power–law relationship represented by Eq. (3):

$$\rho = c(f - f_p)^{-t} \quad (3)$$

in which c is a constant, t a critical exponent, ρ the resistivity, f the fraction of the conductive medium and f_p the fraction at the percolation threshold, expressed as a weight fraction [9,20,27]. From the fitting of the experimental data, f_p and t values of 4 wt% and 1.1, respectively, have been found. The percolation threshold observed in this study is quite similar to that reported for the PVDF/PANI.DBSA blend [24], but it is much lower than that observed on SEBS/PANI.DBSA and SEBS/PPy.DBSA blends [9,20]. This behavior is probably induced by the good compatibility between PVDF and PPy components that induces a conducting network formation into PVDF matrix at very low PPy concentration.

Fig. 2 shows the FTIR spectra of PPy, PVDF and PVDF/PPy blends prepared by solution casting method. The absorption bands at 1520 cm^{-1} and 1424 cm^{-1} in the PPy spectrum can be assigned to the C—C and C—N stretching vibration of pyrrole ring, respectively [27,28]. The absorption band at 1275 cm^{-1} is assigned to C—H or C—N in-plane deformation modes [29], while that those at 1121 and 1015 cm^{-1} are assigned to the C—H bending modes. The absorption band at 1076 cm^{-1} corresponds to the mode in-plane

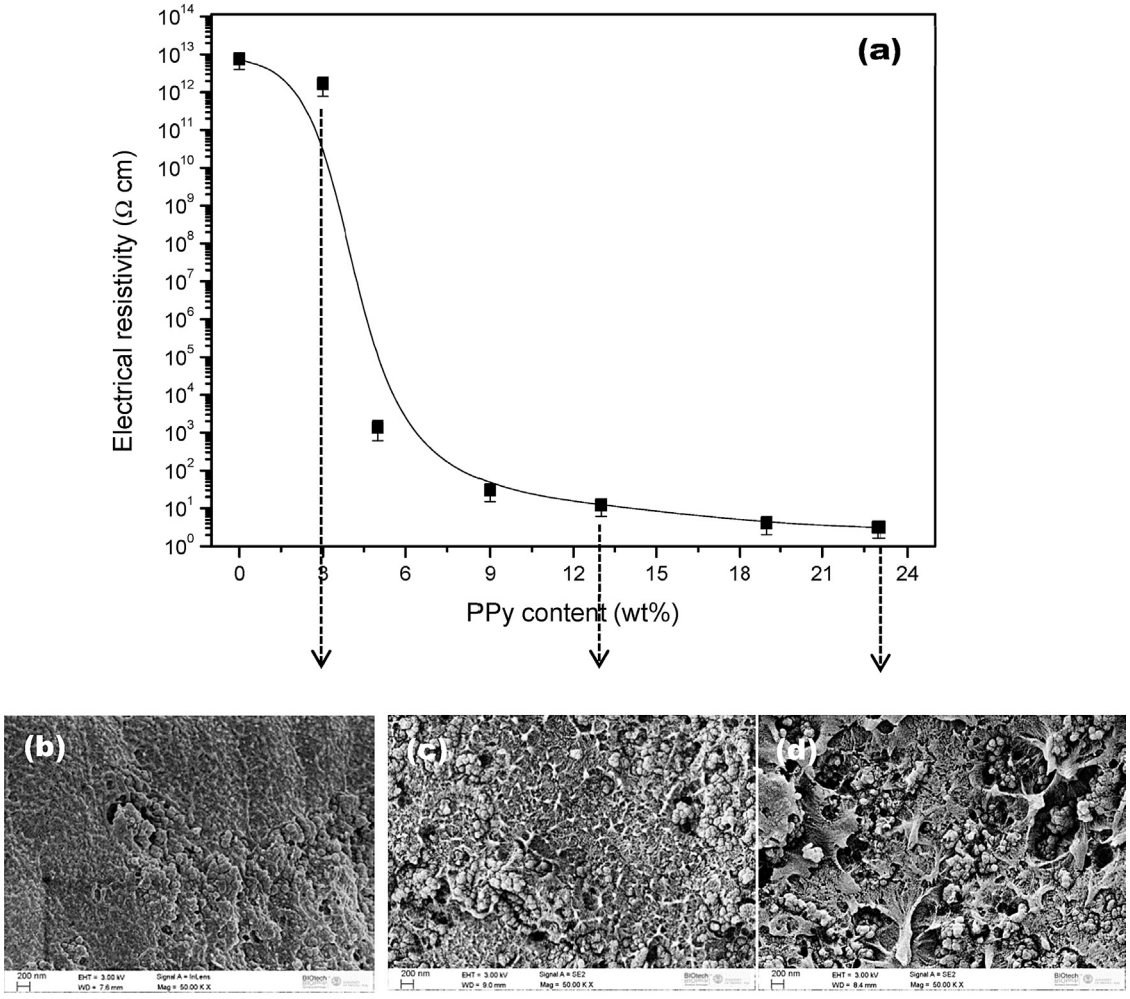

Fig. 1. (a) Effect of PPy content on the electrical conductivity of PVDF/PPy blends. FESEM micrographs of (b) PVDF/PPy_3, (c) PVDF/PPy_13 and (d) PVDF/PPy_23.

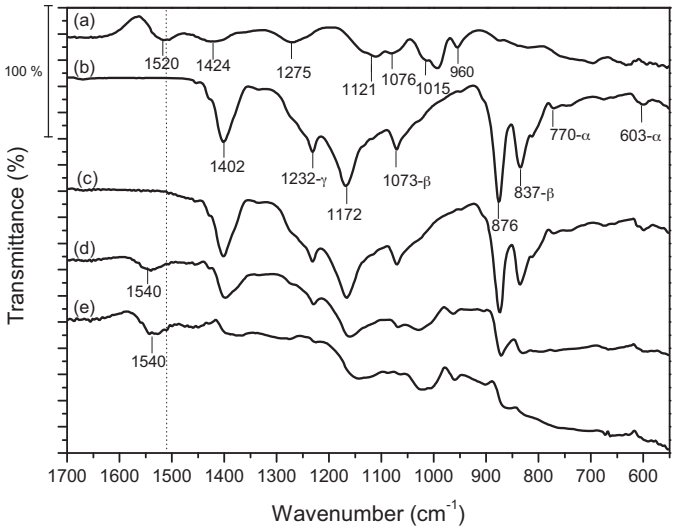

Fig. 2. FTIR spectra of (a) PPy, (b) PVDF, (c) PVDF/PPy_3, (d) PVDF/PPy_13 and (e) PVDF/PPy_23.

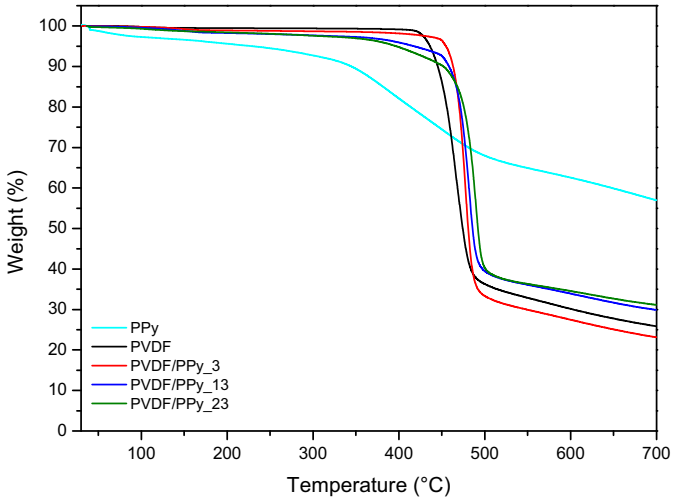

Fig. 3. TGA curves of PVDF film, PPy, PVDF/PPy_3, PVDF/PPy_13 and PVDF/PPy_23.

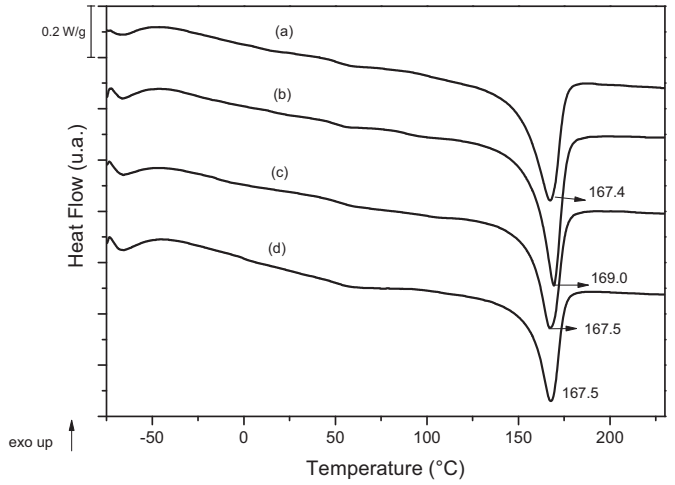

Fig. 4. DSC curves of (a) PVDF, (b) PVDF/PPy_3, (c) PVDF/PPy_13 and (d) PVDF/PPy_23.

deformation vibration of N^+H_2 for doped PPy. The band centered at 965 cm^{-1} is related to the C—H out-of-plane deformation of pyrrole ring [27,28]. PVDF film spectrum showed absorption bands at 1402 and 876 cm^{-1} (band for amorphous phase) attributed to the C—F stretching vibration and at 1172 cm^{-1} assigned to the C—C bond [30–32]. The bands at 837 and 1073 cm^{-1} are associated with the β phase [26,32–34]. The bands at 603 and 770 cm^{-1}, are characteristics of α phase and at 1232 cm^{-1} of γ phase [32]. The PVDF/PPy blend with 3 wt% of PPy showed the predominance of PVDF absorption bands, however, increasing PPy content, the blends exhibited overlapped absorption bands of both PPy and PVDF. Nevertheless, the absorption band at 1520 cm^{-1} for pure PPy are blue-shifted to 1540 cm^{-1} (dashed lines) for blends prepared with 13 and 23 wt% of PPy. The observed absorption band shift can be attributed to the dipole/dipole secondary interaction between —C—F group of PVDF and —N—H group of PPy [35]. These dipole or Van der Waals interactions can affect the stability of the polymers and blend compatibility [35], supporting the idea that the PPy pathway formation into PVDF matrix at very low percolation threshold could be attributed to the chemical interaction of both components.

The effect of PPy addition on the thermal stability of PVDF/PPy blends has also been investigated using thermal gravimetric analyses (TGA), as shown in Fig. 3. Neat PPy presents a weight loss above 320 °C that corresponds to the polymer chain degradation. For the pure PVDF a weight loss is observed at 465 °C, which is attributed to the polymer chain decomposition [36,37]. The blends prepared with various PPy contents start to decompose at higher temperatures than neat PVDF film, e.g. the maximum decomposition temperature shifts from 465 °C to 476 °C, 481 °C and 489 °C for PVDF/PPy blends containing 0, 3, 13 and 23 wt% of PPy, respectively. This behavior can also be attributed to interactions between PVDF and PPy, as observed by FTIR.

Fig. 4 shows the DSC curves of neat PVDF and PVDF/PPy blends with various PPy content. For the neat PVDF the endothermic peak at 167.5 °C can be attributed to the melting of the crystalline phase [38]. The PVDF melting temperature for the PVDF/PPy blends is observed at around the same value.

Table 1 shows the melting temperature (T_m), the sample fusion enthalpy (ΔH_f) and the crystallinity (X_c) of PVDF and PVDF/PPy blends. The PVDF film displays a crystallinity degree of 49.3%, similar to the value reported by Gomes, Serrado Nunes, Sencadas and Lanceros-Mendez [39]. The crystallinity of PVDF/PPy blends is quite similar to the neat PVDF evidencing that the presence of PPy domains does not affect the crystallization of PVDF chains significantly.

The results of dynamical mechanical thermal analysis (DMTA) are presented in Fig. 5. In particular, Fig. 5(a) reports the storage modulus (E′) as a function of temperature for pure PVDF and PVDF/PPy blends. At temperatures below PVDF glass transition temperature ($T_g = -38$ °C), the storage modulus of the blends is lower than that found for the neat PVDF. Above this temperature, the blends are slightly more rigid than neat PVDF. This behavior can be attributed to the stiffening effect of PPy domains and PVDF/PPy blends is illustrated in Fig. 5(b). The PVDF film shows two transition temperatures at around −5 °C and above 50 °C, corresponding to the glass transition and relaxation process associated with molecular motions within the crystalline fraction, respectively [40,41]. On the other hand, for the PVDF/PPy blends, three relaxations are

Table 1
The melting temperature (T_m), melting enthalpy (ΔH_f) and crystallinity content (X_c) of the PVDF and PVDF/PPy with various PPy content.

Sample	Melting peak—T_m (°C)	ΔH_f (J g^{-1})	X_c (%)
PVDF	167.4	51.7	49.4
PVDF/PPy_3	169.0	54.3	53.4
PVDF/PPy_13	167.5	45.2	49.6
PVDF/PPy_23	167.5	40.6	50.3

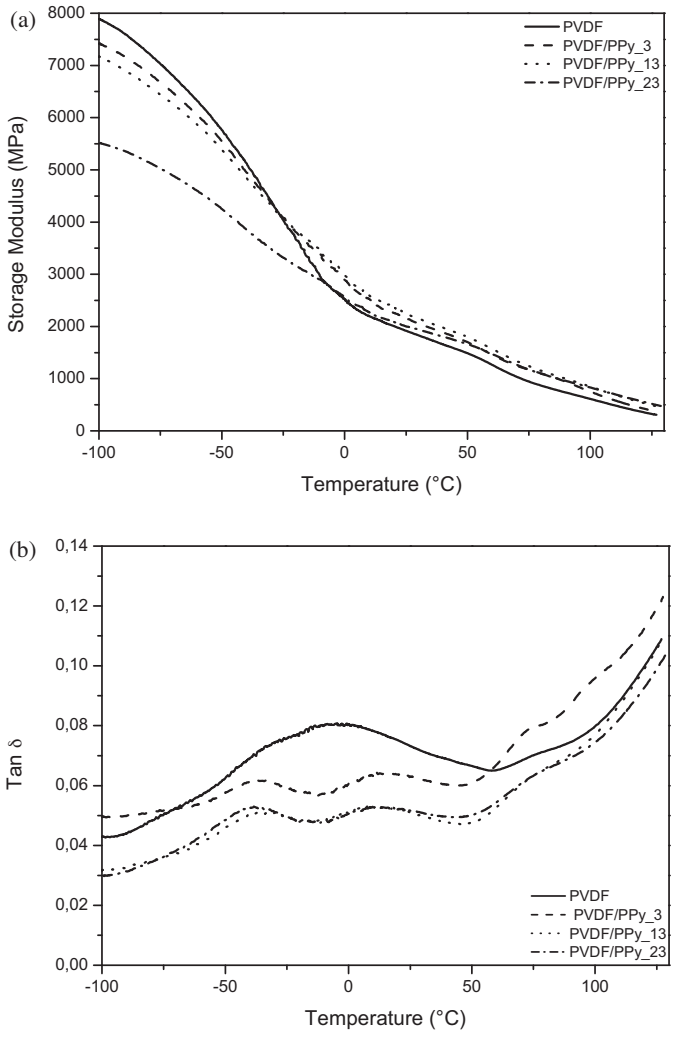

Fig. 5. DMTA traces (a) storage modulus and (b) loss factor films of neat PVDF and PVDF/PPy blends with various PPy content.

detected in all experiments. The two transition temperatures at around −38 °C and 14 °C, are related to the primary relaxation process (glass transition temperature) and secondary process (γ relaxation), respectively [42]. Above 50 °C, the relaxation process can be associated to the molecular motions within the crystalline fraction [40,41]. Additionally, the tan δ intensity reduces significantly on increasing the amount of PPy [20].

Fig. 6 shows the dependence of the electrical resistivity of PVDF/PPy blends during five consecutive loading and unloading cycles under compression. The electromechanical measurements were performed for the blends containing up to 23 wt% of polypyrrole. Due to its highly insulating behavior, the electrical resistivity of neat PVDF does not change when the compressive stress is applied. The PVDF/PPy_3 blend did not display variation in the electrical resistivity during the electromechanical tests. This clearly indicates that at this composition the PPy domains are completely isolated in matrix and the applied compressive stress do not form a conducting network. The blend containing 5 wt% of PPy displayed slightly variation on the electrical resistivity when compressive stress was applied however, the response is not uniform. On the other hand, for blends with 9 wt% PPy content (Fig. 6(a)), the electrical resistivity decreases by two orders of magnitude (from 10^8 to 10^6 Ω cm), probably due to the conducting pathway re-organization and the matrix elastic deformation. When the pressure is released the electrical resistivity returns to almost the original level. For the blends

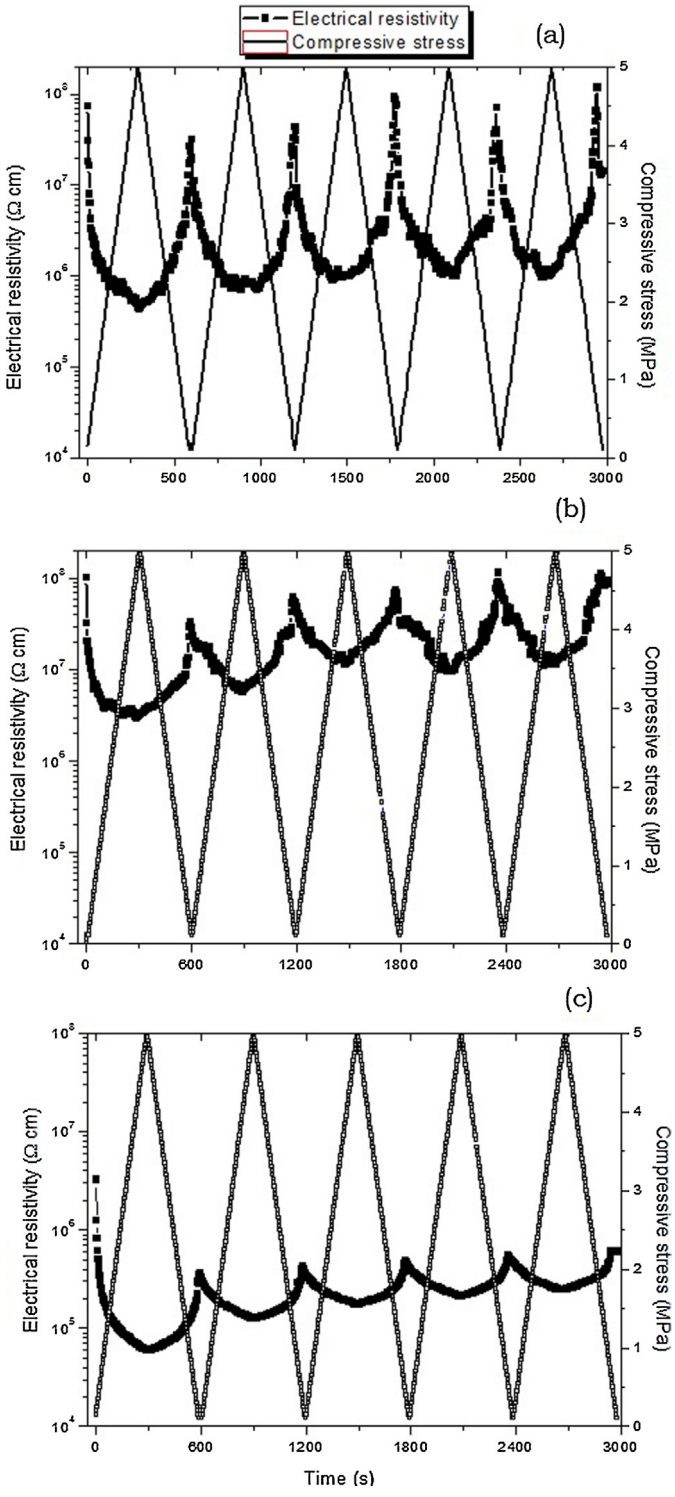

Fig. 6. Electrical resistivity as a function of compressive loading–unloading stress cycles on films of (a) PVDF/PPy_9 (b) PVDF/PPy_13 and (c) PVDF/PPy_23.

with PPy content of 13 wt% and 23 wt% the electrical resistivity changes are less pronounced (Fig. 6(b and c)). This behavior suggests that the PPy domains are very close to each other to be only slightly influenced by the compressive stress applied. Additionally, for these blends there are a variation in the electrical response from the first to the others cycles probably due to the high amount of PPy domains that cannot take advantage of the elastic recovery after load removal.

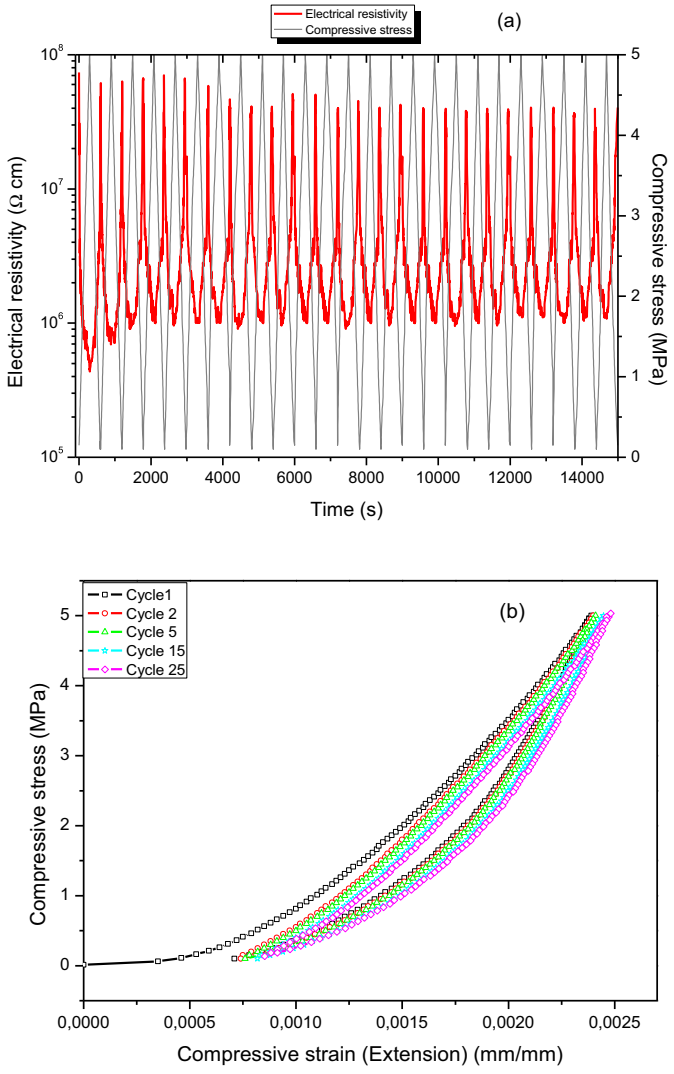

Fig. 7. (a) Electrical resistivity as function of compressive stress during 25 loading and unloading cycles. (b) Compressive stress as function of compressive strain during 25 cycles. Data referred to the PVDF/PPy_9 blends.

Fig. 7(a) shows the dependence of the electrical conductivity on compressive stress during 25 consecutive compressive loading–unloading stress cycles for the blend with 9 wt% PPy content. It is possible to observe a slight difference between the first and the second cycles probably related to the sample accommodation between the electrodes, as shown in the stress–strain curves (Fig. 7(b)). During subsequent cycles the sample presents a small reduction in the variation magnitude of electrical resistivity due to the irreversible deformation. This irreversibility and hysteresis under compressive stress may be explained in terms of destruction of conductive networks during compression and/or matrix plastic deformation [43]. The hysteresis effect can be observed on the stress–strain curves (Fig. 7(b)) that show a residual irreversible strain after 25 cycles.

The electrical resistivity changes under compressive stress detected for the PVDF/PPy blends obtained through solution casting method are about two orders of magnitude. This electrical resistivity changes are higher than the values reported in the open scientific literature for non-conducting matrices containing conducting polymers [8,9,20,24]. Additionally, it is interesting to note that in this work, higher variation of the electrical resistivity were obtained with lower weight fraction of conducting polymer (9 wt%), when compared with others blends described in the open literature [8,9,20,24]. SBS/PANI blends displayed changes on the electrical resistivity from 5.0×10^6 to $1.0 \times 10^6\ \Omega$ cm when the matrix was filled with 30 wt% of PANI [8]. For PVDF/PANI system [24] the highest sensitivity (around one order of magnitude) was obtained for blends with a PANI weight fraction of 10 wt%. In SEBS/PANI.DBSA blends [9], changes on the electrical resistivity are detected only when 30 wt% of PANI.DBSA was incorporated in matrix with variation ranging from 1.0×10^3 to $5.0 \times 10^3\ \Omega$ cm. For SEBS/PPy.DBSA blends [20] the system exhibited variation on the electrical resistivity on pressure loading only after 25 wt% of conducting polymer.

4. Conclusions

In this study a conductive polymer blend constituted of polypyrrole and PVDF through solution casting method was successfully fabricated. The addition of PPy in the PVDF matrix reduces significantly the electrical resistivity at low weight fractions of PPy (5 wt%). With increasing the PPy concentration, the electrical resistivity of PVDF/PPy blends decreases abruptly ten orders of magnitude, reaching a similar value of neat PPy at around 13 wt% of PPy. Electromechanical response was dependent of PPy amount in the blend. Blends with 9 wt% of PPy presented the highest variation (2 orders of magnitude) in the electrical resistivity when compressive stress was applied. It was also observed that by increasing the number of loading-unloading cycles, a slight shift in the electrical resistivity profiles is observed. The electrical resistivity changes of PVDF/PPy films are higher than others conventional systems, which makes these blends suitable materials for pressure sensor devices.

Acknowledgements

GMOB and CM gratefully acknowledge the financial support by Conselho Nacional de Desenvolvimento Científico e Tecnológico (CNPq) grant number 304090/2013 and “Science Without Borders Program - CNPqgrant number 237632/2012-8. The authors also gratefully acknowledge the finantial support by Fundação de Amparo à Pesquisa e Inovação do Estado de Santa Catarina (FAPESC) temo de outorga 2012000067.

References

[1] C. Chang, V.H. Tran, J. Wang, Y.K. Fuh, L. Lin, Nano Lett. 10 (2010) 726–731.
[2] L. Persano, C. Dagdeviren, Y. Su, Y. Zhang, S. Girardo, D. Pisignano, Y. Huang, J.A. Rogers, Nat. Commun. 4 (2013) 1633.
[3] Y. Yang, H. Zhang, G. Zhu, S. Lee, Z.H. Lin, Z.L. Wang, ACS Nano 7 (2013) 785–790.
[4] A.V. Shirinov, W.K. Schomburg, Sens. Actuators, A: Phys. 142 (2008) 48–55.
[5] J. Dargahi, R. Sedaghati, H. Singh, S. Najarian, Mechatronics 17 (2007) 462–467.
[6] M.A. Cullinan, R.M. Panas, C.M. DiBiasio, M.L. Culpepper, Sens. Actuators, A: Phys. 187 (2012) 162–173.
[7] S. Radhakrishnan, S.B. Kar, Sens. Actuators, A: Phys. 120 (2005) 474–481.
[8] F.G. Souza, R.C. Michel, B.G. Soares, Polym. Test. 24 (2005) 998–1004.
[9] G.M.O. Barra, R.R. Matins, K.A. Kafer, R. Paniago, C.T. Vasques, A.T.N. Pires, Polym. Test. 27 (2008) 886–892.
[10] M. Pyo, J.-H. Hwang, Synth. Met. 159 (2009) 700–704.
[11] S. Brady, D. Diamond, K.T. Lau, Sens. Actuators, A: Phys. 119 (2005) 398–404.
[12] A.E. Job, F.A. Oliveira, N. Alves, J.A. Giacometti, L.H.C. Mattoso, Synth. Met. 135–136 (2003) 99–100.
[13] M. Hussain, Y.H. Choa, K. Niihara, Composites A: Appl. Sci. Manuf. 32 (2001) 1689–1696.
[14] D.T. Beruto, M. Capurro, G. Marro, Sens. Actuators, A: Phys. 117 (2005) 301–308.
[15] Y. Ishigure, S. Iijima, H. Ito, T. Ota, H. Unuma, M. Takahashi, Y. Hikichi, H. Suzuki, J. Mater. Sci. 34 (1999) 2979–2985.
[16] S.Y.G.R. Ruschau, R.E. Newnham, J. Appl. Phys. 72 (1992).
[17] K.P. Sau, T.K. Chaki, D. Khastgir, Rubber Chem. Technol. 73 (2000) 310–324.
[18] G.M.O. Barra, M.E. Leyva, B.G. Soares, L.H. Mattoso, M. Sens, J. Appl. Polym. Sci. 82 (2001) 114–123.
[19] M.N. Kalasad, M.A. Gadyal, R.K. Hiremath, I.M. Ikram, B.G. Mulimani, I.M. Khazi, S.K.A. Krishnan, M.K. Rabinal, Compos. Sci. Technol. 68 (2008) 1787–1793.
[20] D. Muller, M. Garcia, G.V. Salmoria, A.T.N. Pires, R. Paniago, G.M.O. Barra, J. Appl. Polym. Sci. 120 (2011) 351–359.
[21] J. Mansouri, R.P. Burford, Polymer 38 (1997) 6055–6069.
[22] N. Bhat, P. Geetha, S. Pawde, Polym. Eng. Sci. 39 (1999) 1517–1524.

[23] A.S. Hutchison, T.W. Lewis, S.E. Moulton, G.M. Spinks, G.G. Wallace, Synth. Met. 113 (2000) 121–127.
[24] S. Radhakrishnan, S.B. Kar, Smart Mater. II 4934 (2002) 23–29.
[25] M. Mičušík, M. Omastová, K. Boukerma, A. Albouy, M.M. Chehimi, M. Trchová, P. Fedorko, Polym. Eng. Sci. 47 (2007) 1198–1206.
[26] N. Wu, Q. Cao, X. Wang, Q. Chen, Solid State Ionics 203 (2011) 42–46.
[27] C. Merlini, B.S. Rosa, D. Müller, L.G. Ecco, S.D.A.S. Ramôa, G.M.O. Barra, Polym. Test. 31 (2012) 971–977.
[28] N.V. Blinova, J. Stejskal, M. Trchová, J. Prokeš, M. Omastová, Eur. Polym. J. 43 (2007) 2331–2341.
[29] M. Omastová, M. Trchová, J. Kovářová, J. Stejskal, Synth. Met. 138 (2003) 447–455.
[30] R. Gregorio, D.S. Borges, Polymer 49 (2008) 4009–4016.
[31] Y.-J. Kim, C.H. Ahn, M.B. Lee, M.-S. Choi, Mater. Chem. Phys. 127 (2011) 137–142.
[32] L. Yu, P. Cebe, Polymer 50 (2009) 2133–2141.
[33] L.M.M. Costa, Mater. Sci. Appl. 01 (2010) 246–251.
[34] E.S. Cozza, O. Monticelli, E. Marsano, P. Cebe, Polym. Int. 62 (2013) 41–48.
[35] S. Saïdi, M. Bouzitoun, A. Mannaî, F. Gmati, H. Derouiche, A.B. Mohamed, J. Phys. D: Appl. Phys. 46 (2013) 355101.
[36] C. Merlini, R.d.S. Almeida, M.A. D'Ávila, W.H. Schreiner, G.M.d.O. Barra, Mater. Sci. Eng., B 179 (2014) 52–59.
[37] Z. Zhong, Q. Cao, B. Jing, X. Wang, X. Li, H. Deng, Mater. Sci. Eng., B 177 (2012) 86–91.
[38] K.P. Pramoda, A. Mohamed, I. Yee Phang, T. Liu, Polym. Int. 54 (2005) 226–232.
[39] J. Gomes, J. Serrado Nunes, V. Sencadas, S. Lanceros-Mendez, Smart Mater. Struct. 19 (2010) 065010.
[40] V. Sencadas, S. Lanceros-Méndez, J.F. Mano, Thermochim. Acta 424 (2004) 201–207.
[41] J.F. Mano, V. Sencadas, A.M. Costa, S. Lanceros-Méndez, Mater. Sci. Eng., A 370 (2004) 336–340.
[42] A. Linares, J.L. Acosta, Eur. Polym. J. 33 (1997) 467–473.
[43] C. Merlini, G.M.O. Barra, T. Medeiros Araujo, A. Pegoretti, RSC Adv. 4 (2014) 15749–15758.